AGU ADVANCING EARTH AND SPACE SCIENCES

Earth and Space Science

RESEARCH ARTICLE
10.1029/2024EA003669

The Post-2020 Surge in Global Atmospheric Methane Observed in Ground-Based Observations

Jennifer Wu[1], Sherry Luo[1], Zhao-Cheng Zeng[2], Debra Wunch[3], Omaira E. García[4], Frank Hase[5], Rigel Kivi[6], Hirofumi Ohyama[7], Isamu Morino[7], Ralf Sussmann[8], Markus Rettinger[8], Yao Té[9], Nicholas M. Deutscher[10], David W. T. Griffith[10], Kei Shiomi[11], Cheng Liu[12,13], Justus Notholt[14], Laura T. Iraci[15], David F. Pollard[16], Thorsten Warneke[14], Coleen Roehl[1], Thomas J. Pongetti[17], Stanley P. Sander[17,†], and Yuk L. Yung[1]

[1]Division of Geological and Planetary Sciences, California Institute of Technology, Pasadena, CA, USA, [2]School of Earth and Space Sciences, Peking University, Beijing, China, [3]Department of Physics, University of Toronto, Toronto, ON, Canada, [4]Izaña Atmospheric Research Center (IARC), State Meteorological Agency of Spain (AEMet), Santa Cruz de Tenerife, Spain, [5]Karlsruhe Institute of Technology (KIT), Institute of Meteorology and Climate Research (IMKASF), Karlsruhe, Germany, [6]Space and Earth Observation Centre, Finnish Meteorological Institute, Sodankyla, Finland, [7]Earth System Division, National Institute for Environmental Studies (NIES), Tsukuba, Japan, [8]Karlsruhe Institute of Technology (KIT), Institute of Meteorology and Climate Research (IMK-IFU), Garmisch-Partenkirchen, Germany, [9]Sorbonne Université, CNRS, MONARIS, UMR8233, Paris, France, [10]Centre for Atmospheric Chemistry, Environmental Futures Research Centre, School of Earth, Atmospheric and Life Sciences, University of Wollongong, Wollongong, NSW, Australia, [11]Earth Observation Research Center, Japan Aerospace Exploration Agency (JAXA/EORC), Tsukuba, Japan, [12]Department of Precision Machinery and Precision Instrumentation, University of Science and Technology of China, Hefei, China, [13]Key Laboratory of Environmental Optics and Technology, Anhui Institute of Optics and Fine Mechanics, Hefei Institutes of Physical Science, Chinese Academy of Sciences, Hefei, China, [14]Institute of Environmental Physics, University of Bremen, Bremen, Germany, [15]Earth Science Division, NASA Ames Research Center, Moffett Field, CA, USA, [16]New Zealand Institute for Earth Science Limited, Lauder, New Zealand, [17]Jet Propulsion Laboratory, California Institute of Technology, Pasadena, CA, USA

Abstract Methane (CH_4) is a potent greenhouse gas with high radiative forcing and a relatively short atmospheric lifetime of around a decade. We used a decade-long data set (2011–2022) from the Fourier transform spectrometer at the California Laboratory for Atmospheric Remote Sensing (CLARS-FTS) to quantify a dramatic increase in methane observed in 2020. We report a significant acceleration of the short-term growth rate of 1.37 ± 0.20 ppb/month starting in 2020 until the end of 2021, a substantial increase relative to the near-zero and negative rates of the preceding 4 years (2016–2019). The observed increase in methane concentrations in 2020 is of significant concern due to its potential contribution to global warming. The Total Carbon Column Observing Network (TCCON) is then used to examine the global geospatial variability of the increase in methane. The results suggest an approximately uniform rise in methane globally. Finally, results from a two-box model used to simulate atmospheric chemical processes of methane production and loss indicate that changes in OH alone are insufficient to explain the rise in atmospheric methane. Recent data from 2022 suggest a deceleration in the methane growth rate, indicating a potential slowdown in the methane increase observed in 2020.

Plain Language Summary In 2020, there was a significant increase in methane, a powerful greenhouse gas. We studied data from 2011 to 2022, specifically using the California Laboratory for Atmospheric Remote Sensing. The methane levels rose sharply in 2020, accelerating by 1.37 parts per billion per month, compared to lower rates from 2016 to 2019. This rise is concerning for global warming. Our global analysis using the Total Carbon Column Observing Network shows a widespread increase in methane. Additionally, our box model results indicate that changes in OH alone can't explain the surge in methane. But there's some good news: the latest data from 2022 shows that the increase in methane might be slowing down.

1. Introduction

Atmospheric methane (CH_4) is a potent greenhouse gas with approximately 80 times the global warming potential of carbon dioxide (CO_2) over a 20-year timeframe (IPCC, 2021). Due to its relatively short atmospheric lifetime of around 10 years, reducing methane emissions can have an immediate effect on slowing global warming. While

[†]Deceased

Key Points:

- Global atmospheric methane increased sharply in 2020; California shows a dramatic increase in methane compared to previous years
- TCCON data shows that the methane rise is approximately uniform globally
- The latest data from 2022 suggest a deceleration in the methane growth rate to the pre-2020 growth rate

Supporting Information:

Supporting Information may be found in the online version of this article.

Correspondence to:

J. Wu,
wu.jennifer3643@gmail.com

Citation:

Wu, J., Luo, S., Zeng, Z.-C., Wunch, D., García, O. E., Hase, F., et al. (2026). The post-2020 surge in global atmospheric methane observed in ground-based observations. *Earth and Space Science*, *13*, e2024EA003669. https://doi.org/10.1029/2024EA003669

Received 4 APR 2024
Accepted 28 JAN 2026

Author Contributions:

Conceptualization: Yuk L. Yung
Data curation: Coleen Roehl, Thomas J. Pongetti
Formal analysis: Jennifer Wu
Funding acquisition: Yuk L. Yung
Investigation: Jennifer Wu, Yuk L. Yung
Methodology: Jennifer Wu, Zhao-Cheng Zeng, Debra Wunch, Stanley P. Sander
Resources: Debra Wunch, Omaira E. García, Frank Hase, Rigel Kivi, Hirofumi Ohyama, Isamu Morino, Ralf Sussmann, Markus Rettinger, Yao Té, Nicholas M. Deutscher, David W. T. Griffith, Kei Shiomi, Cheng Liu, Justus Notholt, Laura T. Iraci, David F. Pollard, Thorsten Warneke, Thomas J. Pongetti, Stanley P. Sander

Software: Sherry Luo
Supervision: Zhao-Cheng Zeng, Yuk L. Yung
Visualization: Jennifer Wu, Sherry Luo, Zhao-Cheng Zeng
Writing – original draft: Jennifer Wu, Sherry Luo
Writing – review & editing: Jennifer Wu, Zhao-Cheng Zeng, Debra Wunch, Yao Té

urban regions, such as the Los Angeles (LA) Basin, have been shown to be major emitters of methane primarily due to leaky natural gas infrastructure (Wennberg et al., 2012; Wunch et al., 2016), the global methane budget is primarily driven by agriculture, wetlands, fossil fuel production, and waste management (Hausmann et al., 2016; Stavert et al., 2022). In an effort to slow down global warming, California implemented Senate Bill 1383 in 2016, mandating a 40% reduction in CH_4 emissions below 2013 levels by 2030.

The year 2020 presented a unique opportunity to study the impact of human activity on atmospheric CH_4. The global COVID-19 pandemic triggered widespread lockdowns, significantly altering human behavior and reducing emissions of various pollutants, including nitrogen oxides (NO_X), CO_2, and CH_4 (e.g., Laughner et al., 2021). However, NOAA's preliminary analysis revealed a surprising outcome: a record-breaking annual increase of 15 ppb in atmospheric CH_4 (Kiest, 2021).

This unexpected surge has ignited debate about the underlying causes. Qu et al. (2022) and Peng et al. (2022) highlighted the role of increased wetland emissions. Feng et al. (2023) further investigated the drivers of this surge, concluding that increased emissions were predominantly responsible, with a significant contribution from reduced OH. Despite these valuable insights, the lack of consensus on the dominant driver for the 2020 anomaly reflects the complexity of methane dynamics (e.g., Sussmann et al., 2012).

While these studies have primarily used inverse modeling techniques to investigate changes in methane emissions, our study offers a complementary approach by directly analyzing atmospheric observations. While inverse modeling studies can provide valuable insights into global and regional emission trends, they are subject to uncertainties in the prior estimates of emissions and atmospheric transport models. In contrast, our analysis of ground-based observations provides a more direct assessment of changes in atmospheric methane concentrations.

We leverage two critical data sets: The California Laboratory for Atmospheric Remote Sensing Fourier Transform Spectrometer (CLARS-FTS) and the Total Carbon Column Observing Network (TCCON). Beginning in 2011, CLARS-FTS provides long-term, continuous measurements of CH_4 capturing the background troposphere above the planetary boundary layer (PBL). This unique perspective allows us to isolate and analyze changes independent of local surface influences. TCCON offers comprehensive CH_4 measurements across multiple global sites, enabling us to investigate the spatial distribution of the 2020 surge and identify potential contributing regions.

While TCCON column measurements include near-surface contributions and are therefore sensitive to local emissions, CLARS-FTS targets the free troposphere, filtering out short-term variability from the PBL. This makes CLARS-FTS particularly valuable for detecting large-scale or hemispheric changes in methane that are less influenced by local sources. Including both data sets allows us to distinguish between regional emission signals and broader shifts in methane sources or sinks.

This study utilizes the comprehensive data sets provided by CLARS-FTS and TCCON to quantify monthly atmospheric methane growth rates at several locations across the globe. Traditionally, atmospheric methane growth rates are reported on an annual basis. The NOAA Global Monitoring Laboratory reports annual increases in atmospheric methane based on globally averaged marine surface sites. The annual increase in atmospheric methane is the increase in its abundance from January 1 of that year to January 1 of the next year after removing its seasonal cycle (Thoning et al., 2022). In contrast, our study reports monthly growth rates to highlight the short-term variations within the specific 2-year period 2020–2021.

By analyzing these data sets and utilizing a box model used to simulate atmospheric chemical processes of methane production and loss, we aim to (a) analyze the spatiotemporal dynamics of the 2020 CH_4 increase, and (b) investigate the potential influence of changes in atmospheric chemistry (e.g., OH concentrations and emissions) to the observed increase.

Our novel approach, combining high-resolution measurements from CLARS-FTS and TCCON, provides valuable insights into the global dynamics of the post-2020 methane surge. By analyzing data from multiple sites, we have identified a widespread increase in methane concentrations across the globe. The widespread nature of the increase emphasizes the need for global efforts to mitigate methane emissions and limit their impact on climate change.

2. Materials and Methods

2.1. CLARS-FTS Data Set

This study utilizes a unique data set from the California Laboratory for Atmospheric Remote Sensing Fourier transform Spectrometer (CLARS-FTS), an instrument operated by NASA's Jet Propulsion Laboratory. Located atop Mt. Wilson, California, at an altitude of 1,673 m, CLARS-FTS offers a vantage point overlooking the LA Basin. It captures near-infrared solar absorption spectra by pointing toward 33 different surface reflection points. These spectra are then converted into column-averaged dry-air mole fractions of various greenhouse gases (XGHG), including carbon dioxide (XCO_2), methane (XCH_4), carbon monoxide (XCO), and nitrous oxide (XN_2O). The measurements have been acquired multiple times daily for each target location since September 2011. For detailed information on the algorithm used for converting slant column densities to dry-air mole fractions and instrument specifications, refer to Fu et al. (2014).

CLARS-FTS operates in two measurement modes: the Spectralon Viewing Observations (SVO) and the Los Angeles Basin Surveys (LABS). The former records the background greenhouse gas concentrations of the free troposphere above the instrument by pointing at a Spectralon target on the rooftop of the observatory, while the latter records scattered infrared radiation from target locations across the viewing area, which spans from the San Fernando Valley (western Los Angeles County) in the west to the Inland Empire (San Bernardino and Riverside Counties) in the east and Orange County in the south. The names and locations of the reflection points are given in Wong et al. (2015). This study utilizes methane data obtained using the SVO mode because PBL emissions captured by the LABS measurements confound the interpretation of the free tropospheric variability. While CLARS-FTS in the Spectralon mode provides measurements above the PBL that are isolated from local processes and can be indicative of background methane dynamics, it's important to note that local emissions, while diluted, can still influence the measurements on longer timescales. Additionally, the CLARS-FTS data is limited to a single site and does not provide a complete perspective on global methane.

CLARS-FTS boasts a high degree of precision and resolution for its CH_4 measurements. Under ideal conditions, it can achieve a precision of 0.3–0.5 ppb for dry-air mole fractions of CH_4. Additionally, its spectral resolution of 0.12 cm^{-1} allows for accurate and detailed identification of spectral features related to atmospheric CH_4 (Fu et al., 2014).

2.2. TCCON Data Set

This study also examines methane data from the Total Carbon Column Observing Network (TCCON), which is a global network of ground-based Fourier transform spectrometers that measure spectra of direct sunlight in the short-wave infrared region of the spectrum. Measurements cannot be taken during conditions of limited sunlight, such as at night or under heavy cloud cover. This limitation is similar to that of the CLARS-FTS, which relies on reflected sunlight.

Total column dry-air mole fractions of CO_2, CO, CH_4, N_2O, and other species are retrieved from the spectra using a software suite called GGG (Wunch et al., 2011), and represent the amount of the species of interest in the atmospheric column above the TCCON site. The GGG open-source software package is used by every station in the network to process data, minimizing biases between sites and ensuring easy dissemination of software improvements throughout the network. GGG utilizes GFIT, the same retrieval algorithm as CLARS-FTS, to derive slant column densities from absorption spectra.

As of 2023, TCCON comprises 30 sites worldwide, including at least one station on every continent except Antarctica and South America. The overall objectives of the TCCON include improving the understanding of the carbon cycle and validating satellite retrievals by providing a reliable and robust ground-based data set that adheres to stringent precision and accuracy requirements.

TCCON instruments also offer high precision and resolution for their methane measurements. Under ideal conditions, they can achieve a precision of 0.1–0.2 ppb for column averaged dry mole fractions of methane. Additionally, their spectral resolution of 0.02 cm^{-1} allows for accurate and detailed retrieval of atmospheric CH_4 information (Wunch et al., 2011).

This study analyzed the CH_4 time series for 20 out of the available TCCON sites because we limited our analyses to sites for which there were at least 5 years of available data, encompassing the period of interest (2020–2021). The 20 TCCON sites span the globe, with clusters in Europe (Bremen, Garmisch, Karlsruhe, Ny-Ålesund, Orléans, Paris, and Sodankylä), North America (East Trout Lake, Edwards, Park Falls, Pasadena, and Lamont), and Asia (Hefei, Rikubetsu, Saga, and Tsukuba). These sites are primarily concentrated in the Northern hemisphere, with three in the Southern hemisphere (Darwin, Lauder, and Wollongong). Within these 20 sites, data gaps can occur due to various reasons, including lack of sunlight (e.g., cloudy conditions or polar night) or instrument malfunctions. On average, approximately 13% of the data record at each TCCON site is missing due to these data gaps. A month is considered to be missing data if no valid CH_4 measurements were obtained during that month for a particular site.

2.3. Removing Seasonal and Underlying Trends

To identify anomalies or deviations that are not accounted for by regular seasonal patterns or long-term trends that are well-documented in literature (He et al., 2019; Zeng et al., 2023), this study employs a methodology to remove the cyclical variations and overall trend of XCH_4 from each time series. A statistical model that consists of a linear component and a seasonal component consisting of harmonic functions is fitted to the data in each XCH_4 time series from 2016 to 2019 to model the underlying trend and seasonal cycle, respectively. The model is given by:

$$M(t) = \alpha_0 + \alpha_1 * t + \beta_1 * \sin(2\pi t) + \beta_2 * \cos\left(\frac{2\pi}{12}t\right) + \beta_3 * \sin\left(\frac{4\pi}{12}t\right) + \beta_4 * \cos\left(\frac{4\pi}{12}t\right) \quad (1)$$

Where t is the sequential month number starting from January 2012 ($t = 0$). Under this indexing, the 2016–2019 baseline period corresponds to $t = 48$ through $t = 95$. α_{0-1} are the coefficients for the linear component, and β_{1-4} are the coefficients for the seasonal component.

The Fourier regression model effectively captures the seasonal and long-term trends in the monthly mean XCH_4 values, as evidenced by the residuals in Figure S2 in Supporting Information S1, which are generally randomly distributed around zero. To ensure the accuracy and relevance of the analysis for the post-2020 period of interest, XCH_4 data from 2016 to 2019 are utilized to capture the conditions preceding the target period. This 4-year period was chosen to provide a robust baseline for modeling the seasonal cycle and underlying trend, reflecting the most recent atmospheric conditions prior to the primary study period (post-2020). The predicted values based on the model, representing the seasonal cycle and underlying trend of methane, are depicted by the red line in Figure 1.

The process of determining and removing the seasonal cycle and underlying trend of methane is repeated for each TCCON station analyzed in this study. The fitted monthly means for each TCCON site are visualized in Figure S1 in Supporting Information S1. By removing these expected variations, the study aims to highlight and investigate deviations from the regular patterns, enabling the identification and examination of anomalous methane concentrations that may be indicative of specific events or emission sources. The standard errors of the fitted model parameters are also calculated.

2.4. Estimating Methane Growth Rates Using Linear Regression

In order to investigate the methane trends beyond the year 2020, a weighted linear regression analysis was conducted, using the standard deviations of each monthly mean as the weights. Growth rates were calculated for three distinct 2-year periods: 2016–2017, 2018–2019, and 2020–2021. For consistency across all TCCON sites and CLARS-FTS, these fixed time periods were utilized to compute the linear regressions. The slopes obtained from these analyses represent the methane growth rate in ppb/month for each location during the respective period. The uncertainties of the linear regression parameters were also calculated.

For the calculation of linear growth rates, certain sites exhibited outliers that were found to disproportionately influence the weighted linear regression, leading to unrepresentative growth rate estimates. These outliers were identified and removed using the Interquartile Range (IQR) method (defined as values falling outside 1.5 times the IQR from the first or third quartile of the monthly anomalies within the respective 2-year period). The impact of this outlier treatment on specific sites is discussed in Section 3.2.

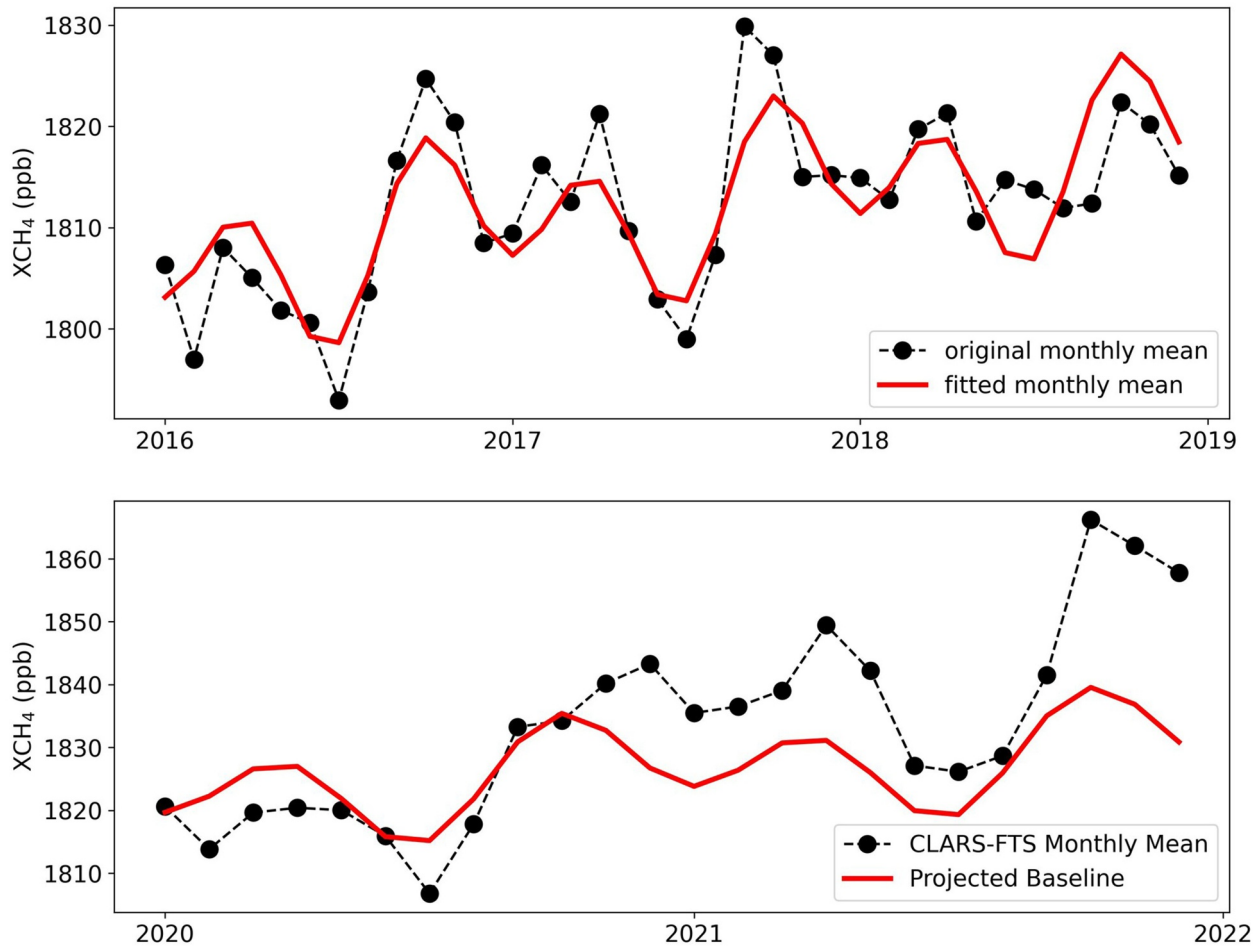

Figure 1. Comparison of original monthly mean data and baseline model fit of methane data from the SVO mode of CLARS-FTS using linear trend and harmonics. (a) Monthly mean observations during the 2016–2019 baseline period (black circles) and the resulting model fit (solid red line) which incorporates a linear trend and seasonal harmonics. (b) Monthly mean observations during the 2020–2021 methane surge period (black circles) compared against the projected baseline model (solid red line). The positive anomalies discussed in Section 3 are calculated as the residuals between the observations in panel (b) and this projected baseline model.

2.5. Box Model

A two-box model (Turner et al., 2019) with the inclusion of a coupled methane–carbon monoxide–hydroxyl radical (CH_4-CO-OH) system (Prather, 1994) was employed here to complement the impacts of changes in OH level on methane. This two-box model incorporates northern and southern hemispheres and simulates annual hemispheric concentrations of target species with a 1-year timescale for inter-hemispheric transport. Associated details of this two-box model, including target species, inversion methods and chemical reactions, can be found in Turner et al. (2017) and Nguyen et al. (2020). Even though some impacts of atmospheric processes cannot be accurately described in the box model, the well-reproduced methane stabilization and renewed growth periods in Turner et al. (2017) still present the advantages of this box model in simulating decadal trends of atmospheric methane and hydroxyl.

Emission data for the model were sourced from the Emissions Database for Global Atmospheric Research (EDGAR) version 4 inventory, a globally recognized data set of anthropogenic and natural emissions. EDGAR provides spatially and temporally resolved estimates of various pollutants, including methane (Muntean et al., 2018).

Thus, in response to the OH level changes resulting from COVID-19 lockdowns, a series of sensitivity tests were conducted using the box model, involving reductions in OH ranging from 2% to 5%. The upper limit of 5% OH reduction was chosen based on previous studies, such as Turner et al. (2017), which have investigated

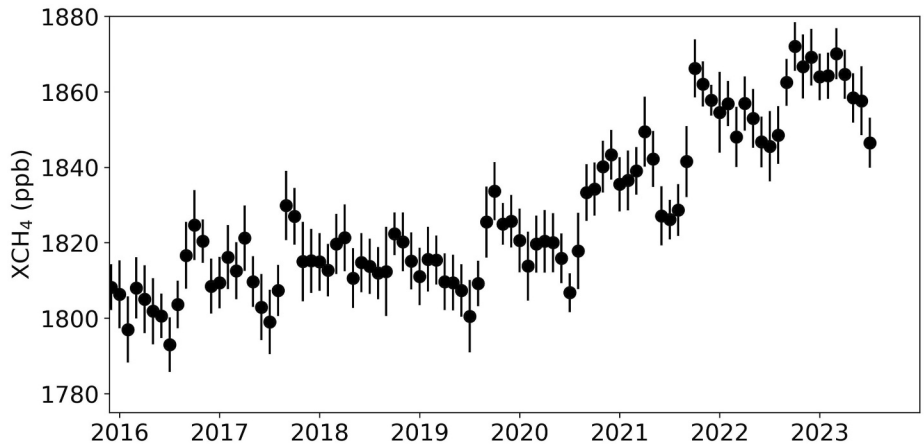

Figure 2. Monthly means of XCH_4 measured by CLARS-FTS in the SVO mode from 2016 to mid-2023. The figure provides a visual representation of the raw data, capturing the natural variability and trends in CH_4 concentrations before any deseasonalization and detrending procedures are applied.

the potential impact of significant perturbations to the OH radical on atmospheric methane. Furthermore, to assess additional impacts of methane emissions, three additional sensitivity tests involving increases in methane emissions (by 10, 20, and 30 Tg) under a fixed 3% reduction in OH were performed (Miyazaki et al., 2021). All tests were conducted for the calendar year 2020, coinciding with the major COVID-19 lockdown periods.

3. Results and Discussion

3.1. CLARS-FTS

Figure 2 depicts the raw monthly means of XCH_4 as captured by CLARS-FTS in the SVO mode, focusing on the period from 2016 onwards, which is relevant to our analysis. For the full operational record of raw monthly mean XCH_4 from CLARS-FTS, spanning from August 2011 to mid-2023, see Figure S3 in Supporting Information S1. The raw data shows a clear seasonal cycle, with peak concentrations in winter and minimums in summer. An upward trend in XCH_4 is also evident throughout the time series. These observed trends and variability form the basis for the deseasonalized and detrended time series analysis presented in Figure 3.

The deseasonalized and detrended XCH_4 time series recorded by CLARS-FTS in the SVO mode is depicted in Figure 3. The full deseasonalized and detrended time series for CLARS-FTS, spanning its entire data record is provided in Figure S4 in Supporting Information S1. The linear regression analysis conducted on the 2020–2021 time period yielded a slope of 1.37 ± 0.20 ppb/month ($p = 5.74 \times 10^{-7}$), indicating a significant positive trend with a correlation coefficient of 0.69. To clarify the interpretation of this value, the 1.37 ± 0.20 ppb/month growth rate represents the rate of change in the anomalies of XCH_4 concentrations, which are derived by removing the seasonal cycle and the underlying trend as described in Section 2.3. Therefore, this value quantifies the additional or accelerated growth rate of methane beyond what would be expected from the pre-existing underlying trend. This growth rate is consistent with the 1.16 ± 0.21 ppb/month growth rate observed at the nearby TCCON site in Pasadena (see Figure 4), falling within the error bars of both measurements. While this consistency indicates strong agreement between the two data sets, it is important to note that TCCON and CLARS-FTS have different viewing geometries. TCCON measures the total atmospheric column above the instrument, encompassing the planetary boundary layer (PBL), while the CLARS-FTS SVO mode measures only the portion above the PBL. This difference could potentially influence the comparison due to varying sensitivities to emission sources within the PBL. There is an increased growth rate in methane of 1.37 ± 0.20 ppb/month during the 2020–2021 time period relative to the linear trend. In contrast, the 2016–2017 and 2018–2019 time periods showed near-zero and negative changes in the methane growth rate respectively. It is worth noting that the rate of increase appears to decrease after 2022.

10.1029/2024EA003669

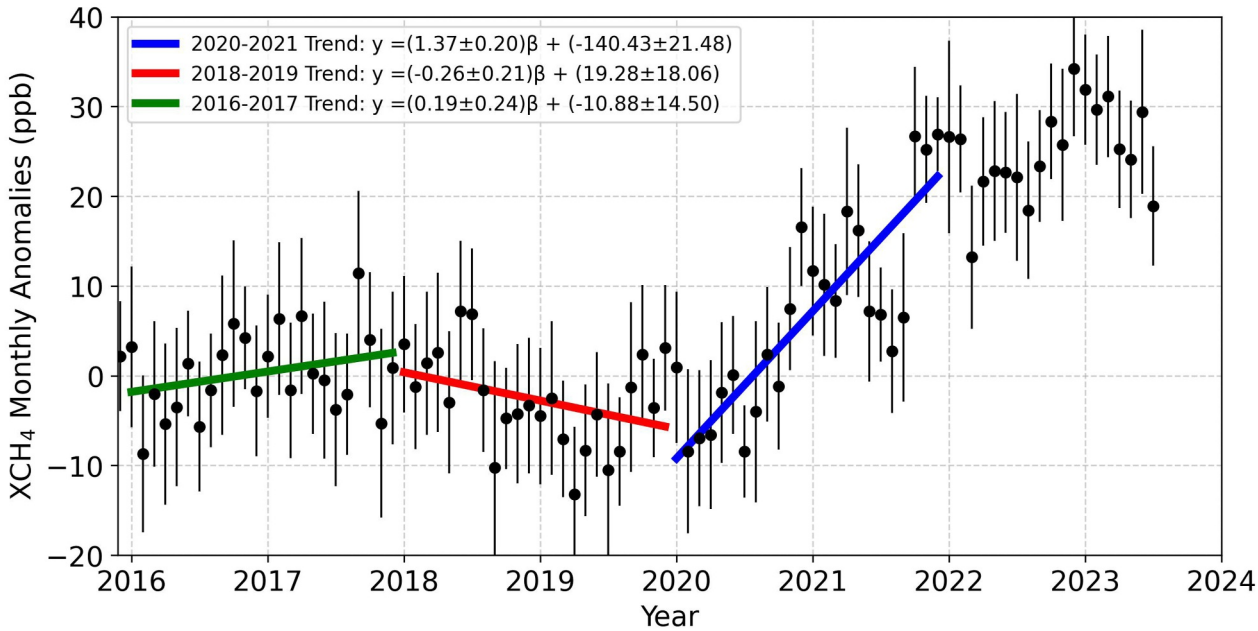

Figure 3. The deseasonalized and detrended time series of methane as measured by CLARS-FTS in the SVO mode. The black circles represent the monthly mean anomaly data with their associated error bars. Monthly anomalies are calculated by removing the underlying trend and seasonal cycle estimated from a Fourier regression fit to data from 2016 to 2019 (see Section 2.3). Error bars represent one standard deviation of the mean. The colored lines show the fitted weighted linear regressions to the monthly mean anomalies for three distinct 2-year periods, as indicated in the legend. All regression parameters are calculated with $t = 0$ starting in January 2012; intercepts in the legend are relative to this date. The fitted slopes and intercepts, along with their uncertainties, are also provided in the legend for each period.

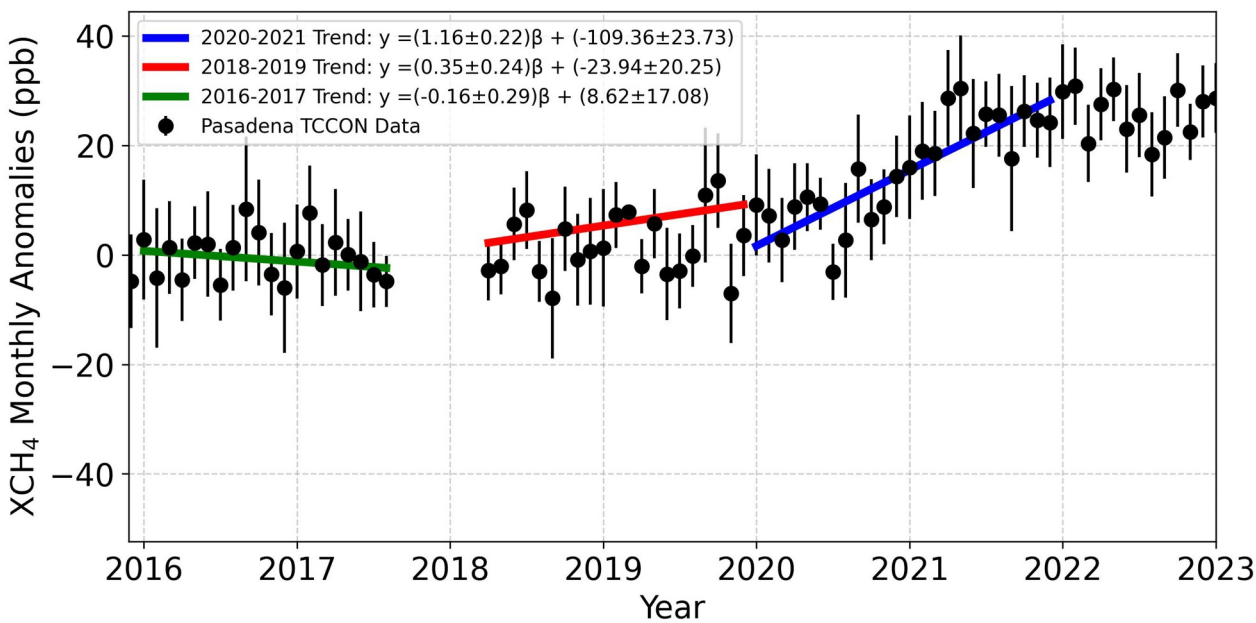

Figure 4. The deseasonalized and detrended time series of CH_4 measured by the TCCON station at Pasadena, California. Monthly anomalies were calculated using the same method described in Figure 3 and Section 2.3. Error bars represent one standard deviation of the mean. The colored lines show the fitted weighted linear regressions to the anomalies for three distinct 2-year periods, as indicated in the legend. The fitted slopes and intercepts, along with their uncertainties, are also provided in the legend for each period.

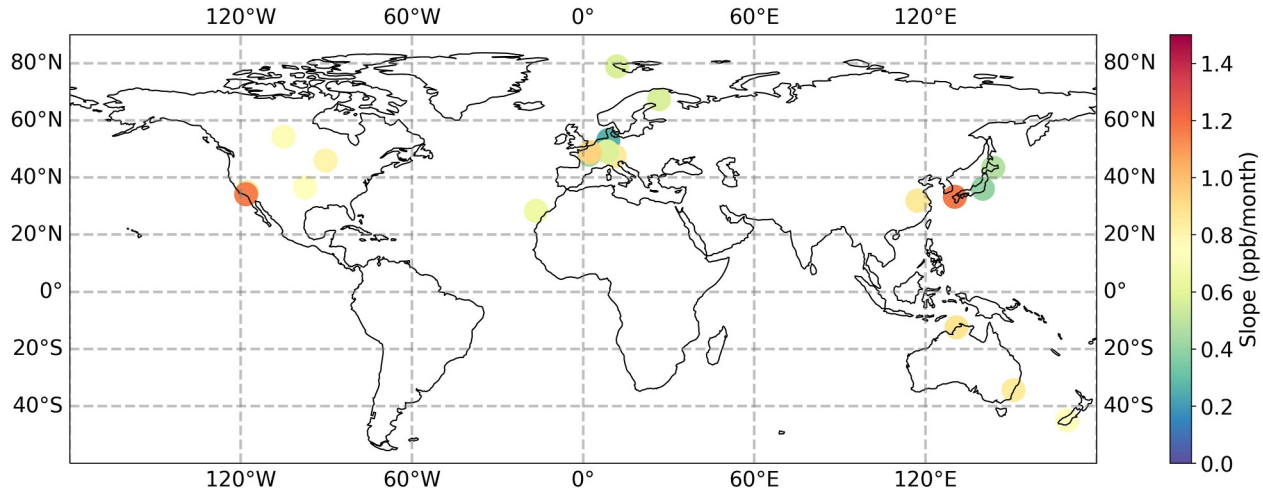

Figure 5. Global distribution of XCH_4 growth rates. The figure displays a world map with color-coded markers representing the methane growth rates derived by the slopes of the linear regression lines fit to data from 2020 to 2021. The colorbar on the right side of the map indicates the range of slope values, ranging from 0 to 1.5 ppb/month.

While the 2020–2021 growth rate, as visualized in Figures S3 and S4 in Supporting Information S1, appears similar in steepness to the overall long-term trend observed from 2011 to 2024, and the 2016–2019 trend was notably flatter, our analysis focuses on the anomalous growth rates relative to the immediate preceding period (2016–2019). The rapid and significant acceleration observed in 2020–2021, following the flatter growth rate observed in 2016–2019 constitutes a "surge" in the context of recent methane dynamics, indicating a substantial deviation from the recent past.

3.2. TCCON

This section explores the global footprint of the post-2020 XCH_4 surge observed in Figure 3. The full deseasonalized and detrended CH_4 time series for the 20 TCCON sites are included in Appendix A. Figure 4 depicts one of these time series after deseasonalizing and detrending for the TCCON station in Pasadena, California.

Figure 4 shows a strong increase in XCH_4 during the 2020–2021 period observed by the TCCON station at Pasadena, California. There is a notable gap in the data record at the end of 2017. The absence of data at the end of 2017 may impact the deseasonalization and detrending analysis because data from 2016 to 2019 are used to perform the fitting. The optimal parameters derived from the Fourier fitting and their associated 1-sigma uncertainties are reported in Table S1 in Supporting Information S1. The same deceleration of the methane surge seen in CLARS-FTS's data starting in 2022 is seen in Figure 4.

Figure 5 presents a world map showcasing the spatial variation of the XCH_4 increase. A zoomed-in view highlighting the methane growth rates observed at the European sites is provided in Figure S5 in Supporting Information S1.

Analysis of the spatial distribution of these growth rates, as presented in Figure 5 and detailed in Table 1, reveals a widespread increase across the TCCON network. While the majority of sites exhibit a notable acceleration in methane growth post-2020, there is some regional variability in the magnitude of this surge. For instance, sites in the Northern Hemisphere mid-latitudes generally show stronger positive anomalous growth rates compared to some Southern Hemisphere sites or those with significant data gaps. The observed patterns highlight the global nature of the post-2020 methane surge, albeit with regional nuances that warrant further investigation.

It is important to note the variability observed at individual sites when evaluating their short-term growth rates. For instance, the TCCON site at Bremen, Germany, initially exhibited an anomalous methane growth rate of −1.43 ppb/month for the 2020–2021 period. As discussed in Section 2.4, extreme negative outliers in Bremen's monthly anomalies (e.g., a residual of −30.39 ppb in March 2021, associated with an unusually small reported uncertainty) were identified and removed prior to re-calculating the 2020–2021 growth rate. This outlier treatment

Table 1
XCH_4 Growth Rates and Uncertainties Estimated by Weighted Linear Regression of 2016–2017, 2018–2019, 2020–2021 Data at Each TCCON Site

Site	Location (Lat, Lon)	2016–17 growth rate (ppb/month)	Uncertainty (ppb/month)	2018–19 growth rate (ppb/month)	Uncertainty (ppb/month)	2020–2021 growth rate (ppb/month)	Uncertainty (ppb/month)	Data reference
Bremen	53.1, 8.85	1.39	1.13	−0.56	0.12	0.28	0.19	Notholt et al. (2023)
Darwin	−12.43, 130.29	−0.22	0.13	−0.22	0.15	0.87	0.23	Deutscher et al. (2024)
East Trout Lake	54.35, −104.99	−0.50	0.32	0.15	0.30	0.74	0.22	Wunch et al. (2023)
Edwards	34.96, −117.88	−0.14	0.36	−0.09	0.28	0.85	0.18	Iraci et al. (2023)
Garmisch	47.48, 11.06	−0.28	0.16	0.18	0.17	1.07	0.15	Sussmann and Rettinger (2023)
Hefei	31.91, 117.17	0.32	0.23	0.38	0.14	0.50	0.18	Liu et al. (2023)
Izaña	28.3, −16.48	0.04	0.09	−0.12	0.11	0.69	0.15	García et al. (2023)
Karlsruhe	49.1, 8.44	0.43	0.14	0.00	0.13	0.53	0.14	Hase et al. (2023)
Lamont	36.5, −108.48	0.11	0.23	0.30	0.25	0.73	0.20	Wennberg et al. (2022)
Lauder	−45.05, 169.68	−0.19	0.20	0.00	0.22	0.83	0.22	Pollard et al. (2024)
Ny Ålesund	78.9, 11.9	−0.03	0.24	0.66	0.25	0.57	0.28	Buschmann et al. (2023)
Orléans	47.97, 2.11	−0.90	0.17	−0.21	0.18	0.44	0.24	Warneke et al. (2024)
Paris	48.85, 2.36	−0.52	0.21	0.33	0.22	0.92	0.16	Té et al. (2023)
Park Falls	45.94, −90.27	−0.08	0.20	0.06	0.20	0.80	0.20	Wennberg et al. (2023)
Pasadena	34.14, −118.13	−0.16	0.29	0.35	0.24	1.16	0.22	Wennberg et al. (2022)
Rikubetsu	43.46, 143.77	0.05	0.17	0.71	0.21	0.48	0.35	Morino et al. (2023a)
Saga	33.24, 130.29	0.01	0.17	−0.06	0.16	1.12	0.22	Shiomi et al. (2023)
Sodankyla	67.37, 26.63	−0.01	0.16	0.51	0.27	0.57	0.20	Kivi et al. (2023)
Tsukuba	36.05, 140.12	−0.14	0.19	0.25	0.18	0.40	0.49	Morino et al. (2023b)
Wollongong	−34.41, 150.88	−0.33	0.32	0.07	0.29	0.84	0.26	Deutscher et al. (2023)

yielded a revised growth rate of 0.28 ± 0.19 ppb/month for Bremen (Table 1, Figure A1), which is a more robust and representative estimate given the site's data characteristics. Similarly, other sites such as Ny Ålesund, Rikubetsu, Orléans, and Tsukuba also exhibit less pronounced increases or even slight decreases in their 2020–2021 anomalous growth rates compared to prior periods. We suggest that this variability at individual sites is most plausibly influenced by the presence of data gaps or irregular sampling within a given 2-year period, which can significantly impact the reliability of the growth rate estimate for individual sites. While other factors such as regional methane dynamics, local sources/sinks, and meteorological conditions may also contribute, data completeness appears to be a key consideration for these specific cases (Figure A1). Despite these localized variations and data limitations, the overall pattern across the majority of the TCCON network consistently points to a notable acceleration in methane growth during the post-2020 period.

Visually, the XCH_4 time series in Appendix A appear to show a potential stabilization or slight decrease in the rate of increase following 2022. However, further analysis and continued monitoring are needed to confirm this observation and determine if this represents a sustained change in the long-term trend. While this study focuses on monthly growth rates, the observed increases are consistent with the global trend reported by NOAA (Kiest, 2021).

3.3. Box Model

In comparison to the deseasonalized and detrended methane data obtained from CLARS-FTS, seasonal trends of the box model results were also removed. This was accomplished using the same Linear Trend and Harmonics approach, also with corresponding data from 2016 to 2019 serving as the conditions preceding the target period.

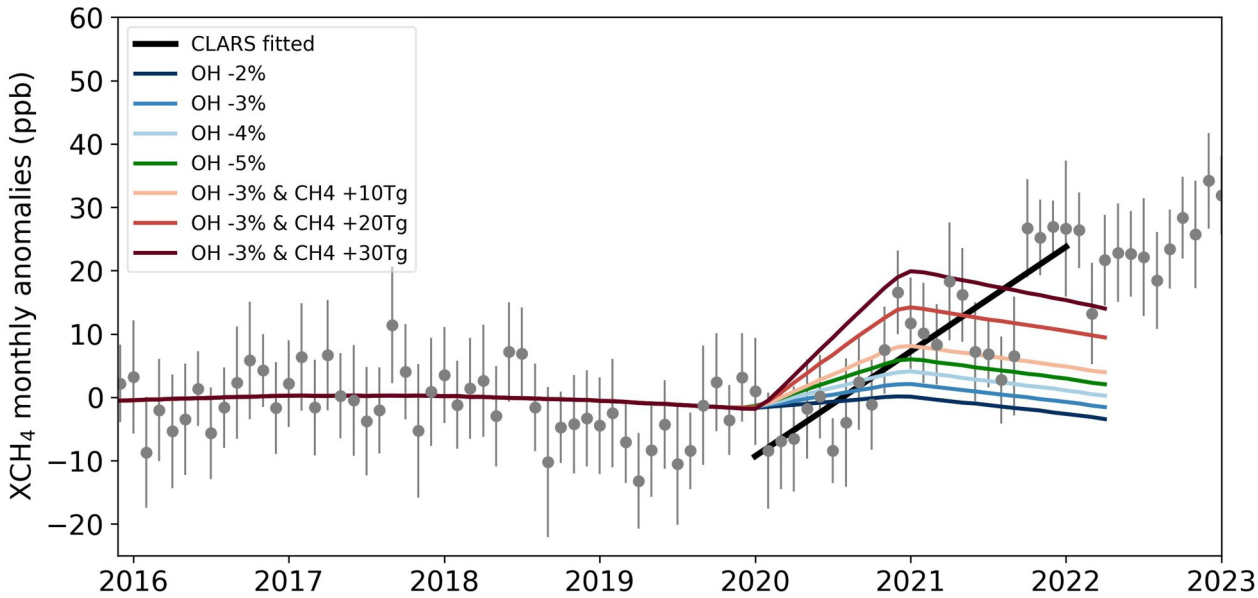

Figure 6. The deseasonalized and detrended time series of methane concentrations from sensitivity tests based on the box model, along with the methane measured by CLARS-FTS in the SVO mode and corresponding linear regression line in black. Monthly anomalies were calculated using the same method described in Figure 3 and Section 2.3.

As shown in Figure 6, overall, increases in methane concentrations are quite noticeable across all sensitivity tests. However, the growth rates vary in different tests. Methane emissions play the dominant role as the greatest increase in emission leads to the highest growth rate in methane. Since the primary removal process for methane is oxidation by hydroxyl radicals (OH), a scenario excluding emissions changes implies that higher methane growth rates would directly correspond to larger decreases in OH levels.

While some of the combined OH-CH_4 scenarios (e.g., "OH −3% & CH_4 +30 Tg") visually resemble the observed increase, their average growth rates remain slightly lower over the full 2020–2021 period. The scenarios tested were selected to span a range of plausible perturbations to OH and CH_4 emissions informed by previous studies. Further exploration of a wider range of combinations—such as increased CH_4 emissions without OH changes or stronger OH reductions—would be valuable in future work.

It is important to note that these simulations were conducted for the period 2020–2021 to specifically investigate the impact of COVID-19 lockdowns on XCH_4. This limited timeframe likely explains why the model shows a decrease in XCH_4 after 2021, whereas the CLARS-FTS data shows a continued increase. Because the simulations do not include any perturbations beyond 2021, the model implicitly assumes a return to pre-pandemic conditions. As a result, it cannot capture any ongoing drivers of methane growth that may have persisted after the lockdown period.

Our ground-based observations from CLARS-FTS and the TCCON network provide robust, direct evidence of the widespread and significant acceleration in atmospheric methane growth rates during the post-2020 period. These observational findings complement recent inverse modeling studies that have investigated the drivers of this surge. For example, our observed anomalous growth rates align with the general increase in global methane emissions inferred by studies such as Qu et al. (2022), Peng et al. (2022), and Feng et al. (2023). While these inverse models primarily attribute the surge to increased emissions from specific source regions (e.g., wetlands in the tropics), Feng et al. (2023) also highlight a significant contribution from reduced OH concentrations, which is consistent with the sensitivity of our box model to OH perturbations. This study offers new insights by providing a comprehensive, ground-based observational perspective that directly quantifies the anomalous growth in atmospheric XCH_4 across a global network. Unlike inverse models that infer emission changes, our direct measurements provide independent validation of the atmospheric response. The consistent acceleration observed across most TCCON sites, despite regional variability and data limitations at some individual sites (as discussed in

Section 3.2), underscores the global nature of this event. Furthermore, our box model sensitivity tests, while simplified, reinforce the notion that a combination of increased emissions and potential changes in the OH sink is necessary to explain the observed magnitude and persistence of the post-2020 methane surge, particularly beyond the initial lockdown period. Future work combining these direct observations with more sophisticated inverse modeling and atmospheric chemistry simulations will be crucial for a more precise attribution of the underlying drivers.

4. Conclusions

We used ground-based observations, CLARS-FTS and TCCON, to investigate the 2020 surge in atmospheric CH_4 concentrations. CLARS-FTS recorded a strong increase in XCH_4 above the planetary boundary layer of 1.37 ± 0.20 ppb/month from 2020 to the end of 2021. Analyses of the CH_4 time series from 20 TCCON sites suggest that the increase in atmospheric XCH_4 was approximately uniform globally. The dramatic rise in XCH_4 was global in scale and not limited to a single region.

Notably, recent data from 2022 suggest a deceleration in this growth rate. This emerging trend highlights the need for continued monitoring to understand the long-term dynamics of atmospheric methane.

Though reductions in OH due to COVID-19 lockdowns may have contributed to the rise in methane during 2020 and beyond, they do not appear to be the sole drivers, as methane concentrations continue to rise even after the lockdown periods in some cases. Our box model results support this idea as decreases in OH alone are not enough to match the rise in methane observed by CLARS-FTS. The approximately uniform global increase in methane aligns with potential causes explored by previous studies, such as reduced OH concentrations and increased wetland emissions, but does not provide definitive evidence to distinguish the relative importance of these factors.

In conclusion, further work needs to be done to untangle the causes behind the dramatic increase in methane. Continued monitoring, integrating more data sets, and utilizing models can add clarity to the factors contributing to the 2020 surge in methane. The response of atmospheric methane to the COVID-19 lockdowns emphasizes the need to consider complex atmospheric chemistry feedbacks when developing and implementing climate change policies.

Appendix A

This appendix includes the full deseasonalized and detrended methane time series for each TCCON station.

10.1029/2024EA003669

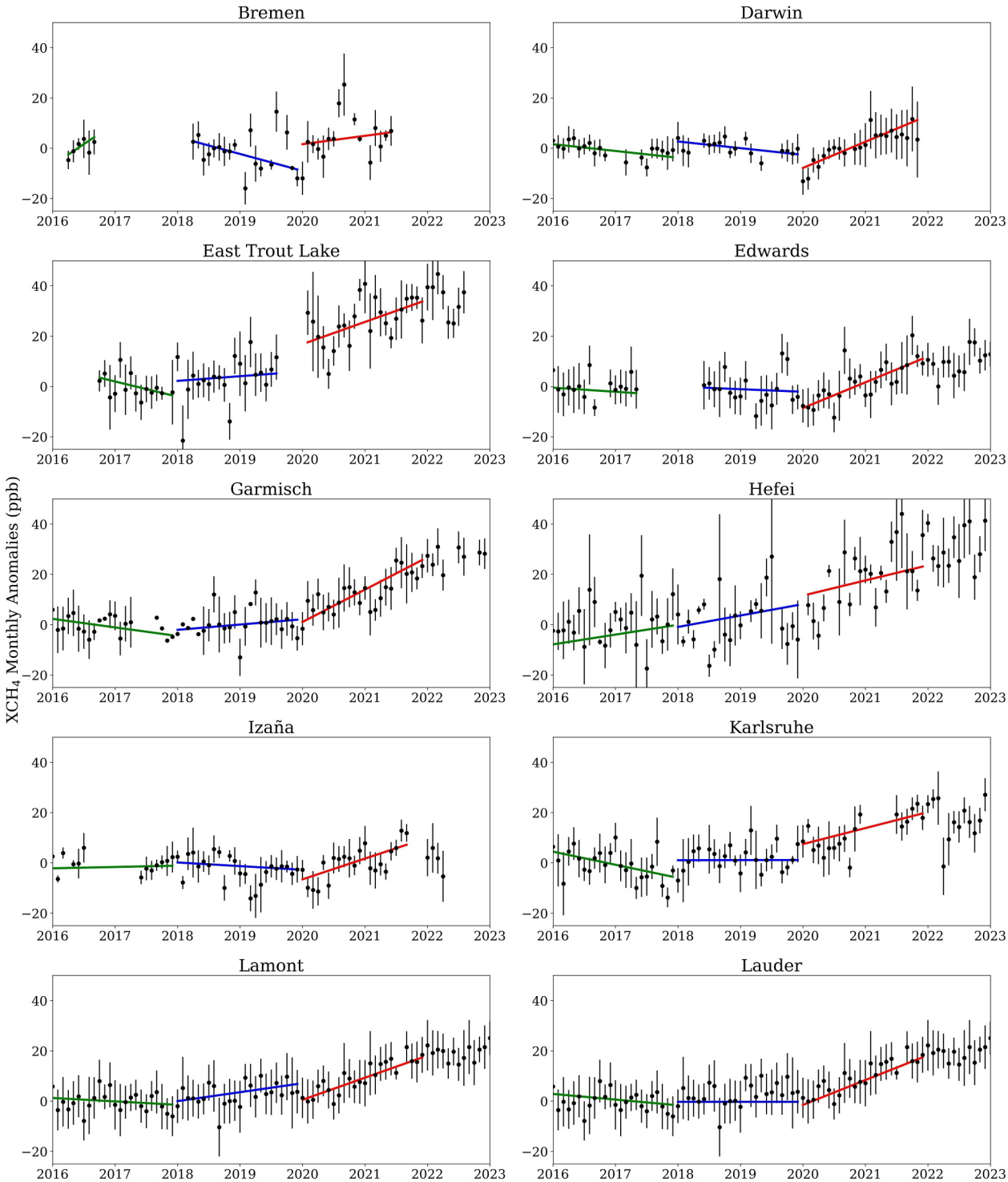

Figure A1. Deseasonalized and detrended XCH_4 monthly anomalies with weighted linear trends for 20 TCCON sites. Each panel depicts monthly mean XCH_4 anomalies (black dots with error bars) for an individual site, labeled accordingly. The green lines represent the weighted linear regressions for the 2016–2017 period, the blue lines for the 2018–2019 period, and the red lines for the 2020–2021 period. These lines highlight the growth rates during these distinct 2-year timeframes. The fitted slopes and their respective uncertainties for all periods are reported in Table 1.

10.1029/2024EA003669

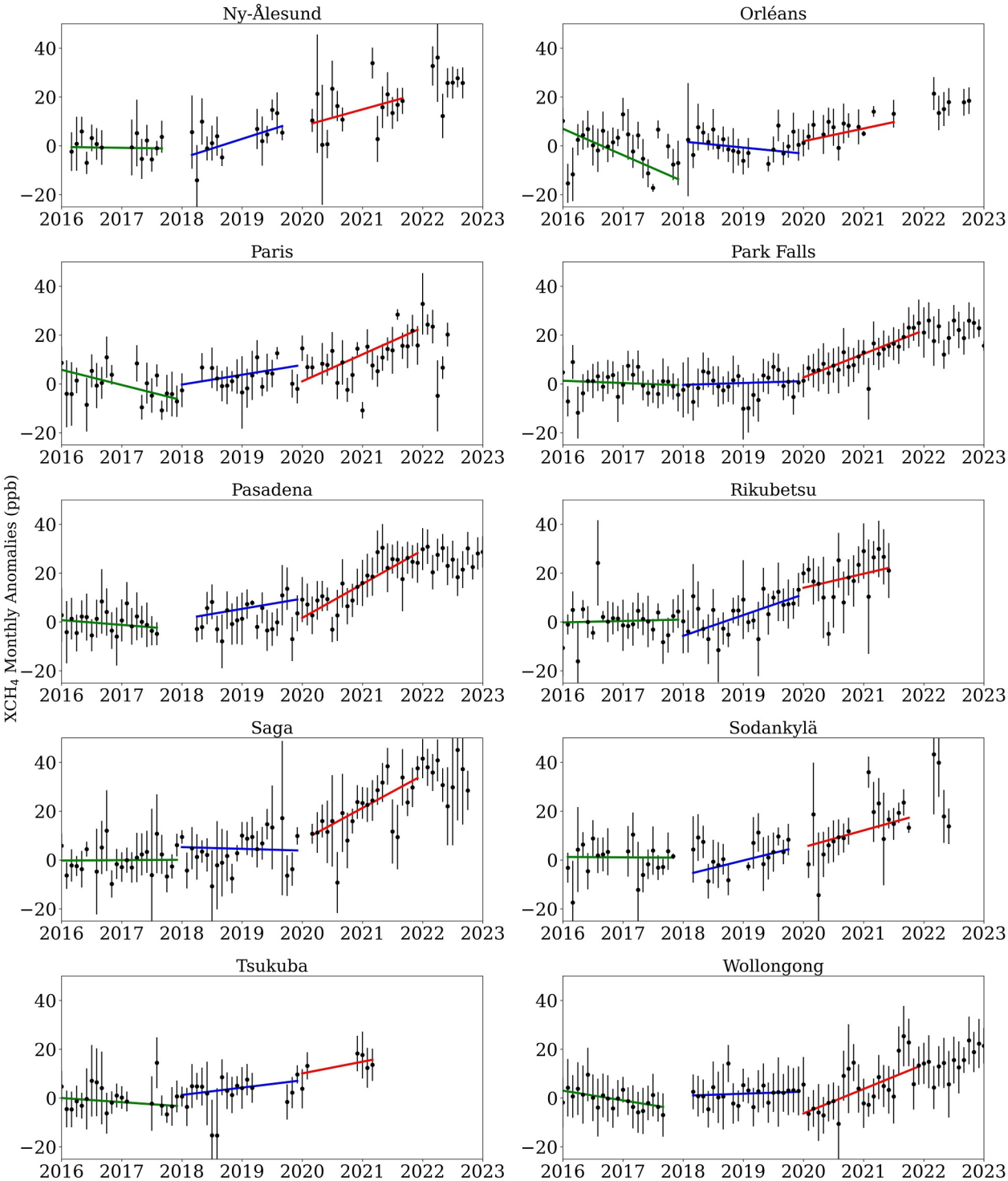

Figure A1. (Continued)

Conflict of Interest

The authors declare no conflicts of interest relevant to this study.

Data Availability Statement

CLARS-FTS XCH_4 data for 2011–2020 are publicly available at https://data.caltech.edu/records/254mc-zpg74 (Sander et al., 2021). TCCON data are available at https://tccondata.org/. The CLARS-FTS Spectralon irradiance data (2011–2023) are available at Zenodo at https://doi.org/10.5281/zenodo.18684558 (Sander et al., 2026).

Acknowledgments
This work is dedicated in part to the memory of Dr. Stanley P. Sander, whose pioneering efforts in atmospheric chemistry and CLARS-FTS development laid the groundwork for this research. We are deeply grateful for his significant contributions and guidance. We also thank Dr. Alex Turner for generously providing the code for the box model used in our sensitivity analysis, which was crucial for investigating the mechanisms driving the methane surge. We acknowledge Paul Wennberg for his instrumental role in securing funding through the Linde Center Grant (GPS.LRFUNDS-3.12-ENDOW. STANBACK) that supported this research. We are also grateful to Paul Wennberg for providing access to TCCON data from the Lamont, Park Falls, and Pasadena sites, and for his valuable comments. The TCCON sites at Rikubetsu and Tsukuba are supported in part by the GOSAT series project. The Paris TCCON site has received funding from Sorbonne Université, the French center CNRS and the French agency CNES. Darwin and Wollongong TCCON stations are supported by ARC Grants DP160100598, LE0668470, DP140101552, DP110103118, and DP0879468 and Darwin through NASA Grants NAG5-12247 and NNG05-GD07G.

References

Buschmann, M., Petri, C., Palm, M., Warneke, T., & Notholt, J. (2023). TCCON data from Ny-Ålesund, Svalbard (NO), Release GGG2020.R0 (Version R0) [Dataset]. *CaltechDATA*. https://doi.org/10.14291/TCCON.GGG2020.NYALESUND01.R0

Deutscher, N. M., Griffith, D. W. T., Paton-Walsh, C., Jones, N. B., Velazco, V. A., Wilson, S. R., et al. (2023). TCCON data from Wollongong (AU), Release GGG2020.R0 (Version R0) [Dataset]. *CaltechDATA*. https://doi.org/10.14291/TCCON.GGG2020.WOLLONGONG01.R0

Deutscher, N. M., Griffith, D. W. T., Paton-Walsh, C., Velazco, V. A., Wennberg, P. O., Blavier, J.-F., et al. (2024). TCCON data from Darwin (AU), Release GGG2020.R0 (Version R0) [Dataset]. *CaltechDATA*. https://doi.org/10.14291/TCCON.GGG2020.DARWIN01.R0

Feng, L., Palmer, P. I., Parker, R. J., Lunt, M. F., & Bösch, H. (2023). Methane emissions are predominantly responsible for record-breaking atmospheric methane growth rates in 2020 and 2021. *Atmospheric Chemistry and Physics*, *23*(8), 4863–4880. https://doi.org/10.5194/acp-23-4863-2023

Fu, D., Pongetti, T. J., Blavier, J.-F. L., Crawford, T. J., Manatt, K. S., Toon, G. C., et al. (2014). Near-infrared remote sensing of Los Angeles trace gas distributions from a mountaintop site. *Atmospheric Measurement Techniques*, *7*(3), 713–729. https://doi.org/10.5194/amt-7-713-2014

García, O. E., Schneider, M., Herkommer, B., Gross, J., Hase, F., Blumenstock, T., & Sepúlveda, E. (2023). TCCON data from Izana (ES), Release GGG2020.R1 (Version R1) [Dataset]. *CaltechDATA*. https://doi.org/10.14291/TCCON.GGG2020.IZANA01.R1

Hase, F., Herkommer, B., Groß, J., Blumenstock, T., Kiel, M., & Dohe, S. (2023). TCCON data from Karlsruhe (DE), Release GGG2020.R1 (Version R1) [Dataset]. *CaltechDATA*. https://doi.org/10.14291/TCCON.GGG2020.KARLSRUHE01.R1

Hausmann, P., Sussmann, R., & Smale, D. (2016). Contribution of oil and natural gas production to renewed increase in atmospheric methane (2007–2014): Top–down estimate from ethane and methane column observations. *Atmospheric Chemistry and Physics*, *16*(5), 3227–3244. https://doi.org/10.5194/acp-16-3227-2016

He, L., Zeng, Z.-C., Pongetti, T. J., Wong, C., Liang, J., Gurney, K. R., et al. (2019). Atmospheric methane emissions correlate with natural gas consumption from residential and commercial sectors in Los Angeles. *Geophysical Research Letters*, *46*(14), 8563–8571. https://doi.org/10.1029/2019GL083400

Intergovernmental Panel on Climate Change (IPCC). (2021). IPCC fifth assessment report: Climate change 2021: The physical science basis. Retrieved from https://www.ipcc.ch/report/ar6/wg1/

Iraci, L. T., Podolske, J. R., Roehl, C., Wennberg, P. O., Blavier, J.-F., Allen, N., et al. (2023). TCCON data from Edwards (US), Release GGG2020.R0 (Version R0) [Dataset]. *CaltechDATA*. https://doi.org/10.14291/TCCON.GGG2020.EDWARDS01.R0

Kiest, K. (2021). Despite pandemic shutdowns, carbon dioxide and methane surged in 2020. Retrieved from https://research.noaa.gov/2021/04/07/despite-pandemic-shutdowns-carbon-dioxide-and-methane-surged-in-2020/

Kivi, R., Heikkinen, P., & Kyrö, E. (2023). TCCON data from Sodankylä (FI), Release GGG2020.R0 (Version R0) [Dataset]. *CaltechDATA*. https://doi.org/10.14291/TCCON.GGG2020.SODANKYLA01.R0

Laughner, J. L., Neu, J. L., Schimel, D., Wennberg, P. O., Barsanti, K., Bowman, K. W., et al. (2021). Societal shifts due to COVID-19 reveal large-scale complexities and feedbacks between atmospheric chemistry and climate change. *Proceedings of the National Academy of Sciences*, *118*(46), e2109481118. https://doi.org/10.1073/pnas.2109481118

Liu, C., Wang, W., Sun, Y., & Shan, C. (2023). TCCON data from Hefei (PRC), Release GGG2020.R0 (Version R0) [Dataset]. *CaltechDATA*. https://doi.org/10.14291/TCCON.GGG2020.HEFEI01.R0

Miyazaki, K., Bowman, K., Sekiya, T., Takigawa, M., Neu, J. L., Sudo, K., et al. (2021). Global tropospheric ozone responses to reduced NO x emissions linked to the COVID-19 worldwide lockdowns. *Science Advances*, *7*(24), eabf7460. https://doi.org/10.1126/sciadv.abf7460

Morino, I., Ohyama, H., Hori, A., & Ikegami, H. (2023a). TCCON data from Rikubetsu (JP), Release GGG2020.R0 (Version R0) [Dataset]. *CaltechDATA*. https://doi.org/10.14291/TCCON.GGG2020.RIKUBETSU01.R0

Morino, I., Ohyama, H., Hori, A., & Ikegami, H. (2023b). TCCON data from Tsukuba (JP), 125HR, Release GGG2020.R0 (Version R0) [Dataset]. *CaltechDATA*. https://doi.org/10.14291/TCCON.GGG2020.TSUKUBA02.R0

Muntean, M., Janssens-Maenhout, G., Song, S., Giang, A., Selin, N. E., Zhong, H., et al. (2018). Evaluating EDGARv4.tox2 speciated mercury emissions ex-post scenarios and their impacts on modelled global and regional wet deposition patterns. *Atmospheric Environment*, *184*, 56–68. https://doi.org/10.1016/j.atmosenv.2018.04.017

Nguyen, N. H., Turner, A. J., Yin, Y., Prather, M. J., & Frankenberg, C. (2020). Effects of chemical feedbacks on decadal methane emissions estimates. *Geophysical Research Letters*, *47*(3), e2019GL085706. https://doi.org/10.1029/2019GL085706

Notholt, J., Petri, C., Warneke, T., & Buschmann, M. (2023). TCCON data from Bremen (DE), Release GGG2020.R0 (Version R0) [Dataset]. *CaltechDATA*. https://doi.org/10.14291/TCCON.GGG2020.BREMEN01.R0

Peng, S., Lin, X., Thompson, R. L., Xi, Y., Liu, G., Hauglustaine, D., et al. (2022). Wetland emission and atmospheric sink changes explain methane growth in 2020. *Nature*, *612*(7940), 477–482. https://doi.org/10.1038/s41586-022-05447-w

Pollard, D. F., Robinson, J., & Shiona, H. (2024). TCCON data from Lauder (NZ), Release GGG2020.R0 (Version R0) [Dataset]. *CaltechDATA*. https://doi.org/10.14291/TCCON.GGG2020.LAUDER03.R0

Prather, M. J. (1994). Lifetimes and eigenstates in atmospheric chemistry. *Geophysical Research Letters*, *21*(9), 801–804. https://doi.org/10.1029/94GL00840

Qu, Z., Jacob, D. J., Zhang, Y., Shen, L., Varon, D. J., Lu, X., et al. (2022). Attribution of the 2020 surge in atmospheric methane by inverse analysis of GOSAT observations. *Environmental Research Letters*, *17*(9), 094003. https://doi.org/10.1088/1748-9326/ac8754

Sander, S., Pongetti, T., Zeng, Z.-C., Wu, J., & Yung, Y. (2026). CLARS-FTS Spectralon XGHGs (2011–2023) [Dataset]. *Zenodo*. https://doi.org/10.5281/ZENODO.18684558

Sander, S., Pongetti, T., Zeng, Z.-C., & Yung, Y. (2021). CLARS-FTS XGHGs Dataset (2011-2020) (Version 1.0) [Dataset]. *CaltechDATA*. https://doi.org/10.22002/D1.1985

Shiomi, K., Kawakami, S., Ohyama, H., Arai, K., Okumura, H., Ikegami, H., & Usami, M. (2023). TCCON data from Saga (JP), Release GGG2020.R0 (Version R0) [Dataset]. *CaltechDATA*. https://doi.org/10.14291/TCCON.GGG2020.SAGA01.R0

Stavert, A. R., Saunois, M., Canadell, J. G., Poulter, B., Jackson, R. B., Regnier, P., et al. (2022). Regional trends and drivers of the global methane budget. *Global Change Biology*, *28*(1), 182–200. https://doi.org/10.1111/gcb.15901

Sussmann, R., Forster, F., Rettinger, M., & Bousquet, P. (2012). Renewed methane increase for five years (2007–2011) observed by solar FTIR spectrometry. *Atmospheric Chemistry and Physics*, *12*(11), 4885–4891. https://doi.org/10.5194/acp-12-4885-2012

Sussmann, R., & Rettinger, M. (2023). TCCON data from Garmisch (DE), Release GGG2020.R0 (Version R0) [Dataset]. *CaltechDATA*. https://doi.org/10.14291/TCCON.GGG2020.GARMISCH01.R0

Té, Y., Jeseck, P., & Janssen, C. (2023). TCCON data from Paris (FR), Release GGG2020.R0 (Version R0) [Dataset]. *CaltechDATA*. https://doi.org/10.14291/TCCON.GGG2020.PARIS01.R0

Thoning, K., Dlugokencky, E., Lan, X., & NOAA Global Monitoring Laboratory. (2022). Trends in globally-averaged CH_4, N_2O, and SF6 [Dataset]. *NOAA GML*. https://doi.org/10.15138/P8XG-AA10

Turner, A. J., Frankenberg, C., & Kort, E. A. (2019). Interpreting contemporary trends in atmospheric methane. *Proceedings of the National Academy of Sciences*, *116*(8), 2805–2813. https://doi.org/10.1073/pnas.1814297116

Turner, A. J., Frankenberg, C., Wennberg, P. O., & Jacob, D. J. (2017). Ambiguity in the causes for decadal trends in atmospheric methane and hydroxyl. *Proceedings of the National Academy of Sciences*, *114*(21), 5367–5372. https://doi.org/10.1073/pnas.1616020114

Warneke, T., Petri, C., Notholt, J., & Buschmann, M. (2024). TCCON data from Orléans (FR), Release GGG2020.R0 (Version R0) [Dataset]. *CaltechDATA*. https://doi.org/10.14291/TCCON.GGG2020.ORLEANS01.R0

Wennberg, P. O., Mui, W., Wunch, D., Kort, E. A., Blake, D. R., Atlas, E. L., et al. (2012). On the sources of methane to the Los Angeles atmosphere. *Environmental Science & Technology*, *46*(17), 9282–9289. https://doi.org/10.1021/es301138y

Wennberg, P. O., Roehl, C. M., Wunch, D., Blavier, J.-F., Toon, G. C., Allen, N. T., et al. (2022). TCCON data from Caltech (US), Release GGG2020.R0 (Version R0) [Dataset]. *CaltechDATA*. https://doi.org/10.14291/TCCON.GGG2020.PASADENA01.R0

Wennberg, P. O., Roehl, C. M., Wunch, D., Toon, G. C., Blavier, J.-F., Washenfelder, R., et al. (2023). TCCON data from Park Falls (US), Release GGG2020.R1 (Version R1) [Dataset]. *CaltechDATA*. https://doi.org/10.14291/TCCON.GGG2020.PARKFALLS01.R1

Wong, K. W., Fu, D., Pongetti, T. J., Newman, S., Kort, E. A., Duren, R., et al. (2015). Mapping CH_4: CO_2 ratios in Los Angeles with CLARS-FTS from Mount Wilson, California. *Atmospheric Chemistry and Physics*, *15*(1), 241–252. https://doi.org/10.5194/acp-15-241-2015

Wunch, D., Mendonca, J., Colebatch, O., Allen, N. T., Blavier, J.-F., Kunz, K., et al. (2023). TCCON data from East Trout Lake, SK (CA), Release GGG2020.R0 (Version R0) [Dataset]. *CaltechDATA*. https://doi.org/10.14291/TCCON.GGG2020.EASTTROUTLAKE01.R0

Wunch, D., Toon, G. C., Blavier, J.-F. L., Washenfelder, R. A., Notholt, J., Connor, B. J., et al. (2011). The total carbon column observing network. *Philosophical Transactions of the Royal Society A: Mathematical, Physical and Engineering Sciences*, *369*(1943), 2087–2112. https://doi.org/10.1098/rsta.2010.0240

Wunch, D., Toon, G. C., Hedelius, J. K., Vizenor, N., Roehl, C. M., Saad, K. M., et al. (2016). Quantifying the loss of processed natural gas within California's South Coast Air Basin using long-term measurements of ethane and methane. *Atmospheric Chemistry and Physics*, *16*(22), 14091–14105. https://doi.org/10.5194/acp-16-14091-2016

Zeng, Z.-C., Pongetti, T., Newman, S., Oda, T., Gurney, K., Palmer, P. I., et al. (2023). Decadal decrease in Los Angeles methane emissions is much smaller than bottom-up estimates. *Nature Communications*, *14*(1), 5353. https://doi.org/10.1038/s41467-023-40964-w